Active Surfaces for Brain Cortex Reconstruction from MR Images

Ph.D. Thesis Proposal

Chenyang Xu
Department of Electrical and Computer Engineering,
The Johns Hopkins University, Baltimore.

February 20, 1997.

ADVISOR: Dr. Jerry L. Prince

1 Introduction

During the last decade, there has been an increasing effort in the medical image analysis community on the subject of reconstructing the human brain cortex from Magnetic Resonance (MR) images. Reconstructing the cortex, however, with its complex geometry of cortical foldings, is a challenging task. Traditional methods based on edge detection and edge linking are computationally intensive and sensitive to noise. Recently, work based on *active surfaces* [1, 2, 3] has shown some promising results. Sandor and Leahy [1] employed active B-spline surfaces, MacDonald *et al.* [2] improved the convergence of active surfaces by using a multi-resolution scheme, and Davatzikos *et al.* [3, 4] modified the external force for active surfaces to allow the active surfaces to find the middle layer of the cortex. These methods, however, are only capable of finding the outer cortex surface or areas where deep convoluted foldings are not present. The drawbacks of these methods are largely due to the two known problems associated with the traditional active surfaces: that they have difficulties moving into concave boundary regions, and that they do not converge to the desired features unless initialized very close to them. These problems are discussed in more detail in Section 3.

In this research, our main objectives are

Objective 1: To design a new active surface model which addresses the two problems associated with the traditional active surfaces.

Objective 2: To reconstruct a complete human brain cortical surface using the proposed new active surface model.

Objective 3: To perform several new applications based on the reconstructed cortical surface.

The research for Objective 1 has been largely completed and published in [5, 6, 7, 8]. Research on Objective 2 is in progress with preliminary results published in [9]. Significant research on Objective 3 has not yet begun.

This proposal is organized as follows. First, in Section 2, we present a traditional active surface model. Next, in Section 3, we demonstrate the problems of traditional active surface models followed by a description of a new active surface model. Several experimental results are shown as well. Then, in Section 4, we introduce a method based on the new active surface model to reconstruct a complete cortical surface. In Section 5, we give an example of computing differential geometry properties on the reconstructed cortical surface. Finally, in Section 6, we discuss the intended directions for future research.

2 Background

The traditional active surface is a parameterized surface $\mathbf{x}(\mathbf{u}) = [x(\mathbf{u}), y(\mathbf{u}), z(\mathbf{u})]^T$, $\mathbf{u} = (u^1, u^2) \in \mathbf{R}^2$, that moves through the spatial domain of a three-dimensional (3D) image to minimize the energy functional

$$E = \int \frac{1}{2}(\alpha \sum_{i=1}^{2} |\mathbf{x}_i|^2 + \beta \sum_{i,j=1}^{2} |\mathbf{x}_{ij}|^2) + E_{ext}(\mathbf{x}) d\mathbf{u} \tag{1}$$

where α and β are weighting parameters that control the surface's tension and rigidity, $\mathbf{x}_i$ and $\mathbf{x}_{ij}$ denote the first and second partial derivatives of $\mathbf{x}$ with respect to u^i, and $E_{ext}(\mathbf{x})$ is the external energy function derived from the image.

Given a gray-level 3D image $I(\mathbf{x})$ (viewed as a function of continuous position variable $\mathbf{x} \in \mathbf{R}^3$), typical external energies designed to lead an active surface toward edges are

$$E_{ext}(\mathbf{x}) = -|\nabla I(\mathbf{x})|^2 \quad \text{or} \tag{2}$$
$$E_{ext}(\mathbf{x}) = -|\nabla(G_\sigma(\mathbf{x}) * I(\mathbf{x}))|^2 \tag{3}$$

where $G_\sigma(\mathbf{x})$ is a 3D Gaussian function with standard deviation σ, ∇ is the gradient operator in $\mathbf{R}^3$, and $*$ is the 3D convolution operator.

Using *calculus of variations* [10], it can be shown that the active surface minimizing E must satisfy the following Euler equation

$$\alpha\nabla^2_{\mathbf{u}}\mathbf{x} - \beta\nabla^2_{\mathbf{u}}(\nabla^2_{\mathbf{u}}\mathbf{x}) - \nabla E_{ext}(\mathbf{x}) = \mathbf{0} \tag{4}$$

where $\nabla^2_{\mathbf{u}} = \frac{\partial^2}{(\partial u^1)^2} + \frac{\partial^2}{(\partial u^2)^2}$ is the Laplacian operator defined in the parameter space. The behavior of Equation (4) can be more readily seen when it is interpreted as a force balance equation

$$\mathbf{F}_{int} + \mathbf{F}_{ext} = \mathbf{0} \tag{5}$$

where $\mathbf{F}_{int} = \alpha\nabla^2_{\mathbf{u}}\mathbf{x} - \beta\nabla^2_{\mathbf{u}}(\nabla^2_{\mathbf{u}}\mathbf{x})$, and $\mathbf{F}_{ext} = -\nabla E_{ext}(\mathbf{x})$. The internal force $\mathbf{F}_{int}$ discourages stretching and bending while the external force $\mathbf{F}_{ext}$ pulls the active surface towards the desired feature.

To find a solution to (4), the active surface is made dynamic by treating $\mathbf{x}$ as a function of time t, as well as u^1 and u^2 — i.e., $\mathbf{x}(u^1, u^2, t)$. Then, the partial derivative of $\mathbf{x}$ with respect to t is then set equal to the left hand side of (4) as follows

$$\mathbf{x}_t = \alpha\nabla^2_{\mathbf{u}}\mathbf{x} - \beta\nabla^2_{\mathbf{u}}(\nabla^2_{\mathbf{u}}\mathbf{x}) - \nabla E_{ext}(\mathbf{x}) \tag{6}$$

When the solution $\mathbf{x}$ stabilizes, the term $\mathbf{x}_t$ vanishes and we achieve a solution of (4).

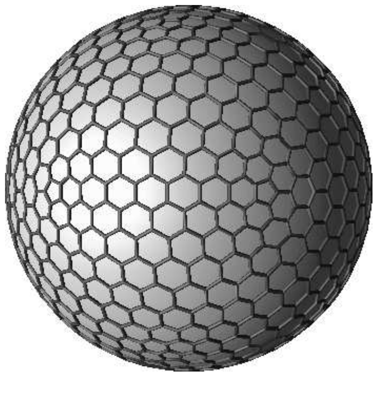

Figure 1: A simplex mesh in 3D.

In order to simulate the active surface on a digital computer, a suitable discretization scheme is required. One attractive discretization scheme is to use *simplex meshes* proposed by Delingette [11]. Simplex meshes always have a fixed number of neighboring vertices for any vertex on the mesh. This property is very useful for designing fast algorithms and makes simplex meshes particularly attractive for reconstructing complex shapes such as the cortical surface. Simplex meshes can be defined in any dimension. An example of a simplex mesh in 3D is shown in Fig. 1. Notice that each vertex on this mesh has exactly three neighboring vertices. Also note that *active contours* are curves in 2D, a two-dimensional analog to active surfaces in 3D. A classical reference on active contours is in [12]. For demonstration purposes, we will use both active surfaces and active contours in the examples throughout this proposal.

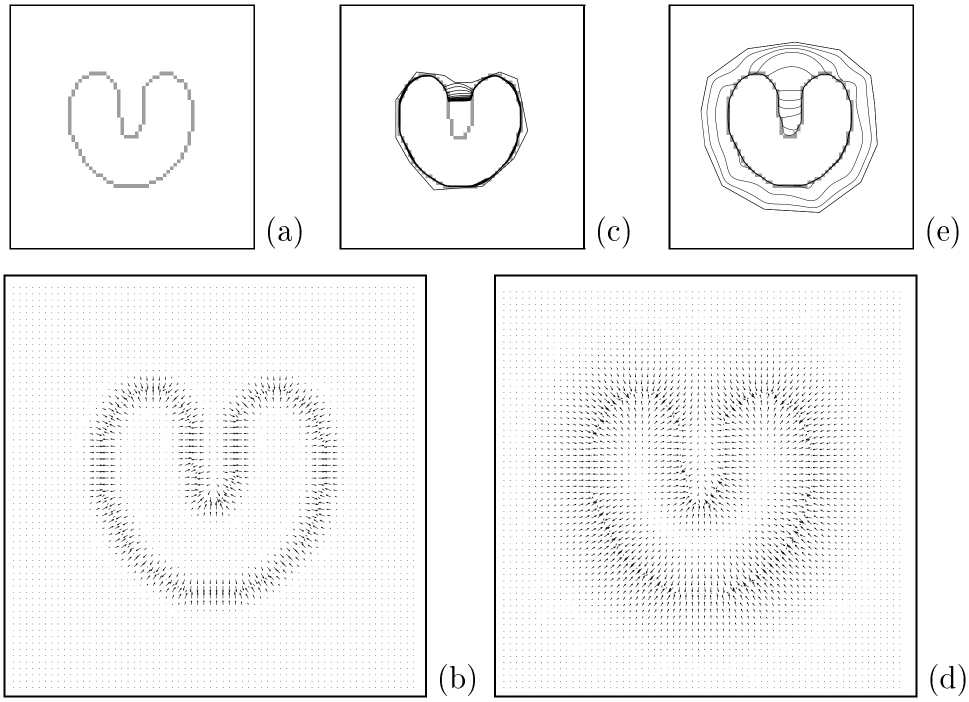

Figure 2: (a) A U-shape object. (b) and (c) An active contour with traditional external forces cannot move into the concave boundary region. (d) and (e) An active contour with GVF external forces moves into the concave boundary region.

3 A New Active Surface Model

3.1 Problems with Traditional Active Surfaces

There are two key difficulties with the traditional active surfaces. First, the initial active surface must, in general, be close to the desired boundary or else it will likely converge to the wrong result. Several methods have been proposed to address this problem including scale-space methods [12] and pressure forces [13]. The basic idea is to increase the "capture range" of the external force fields and to guide the surface toward the desired boundary. The second problem is that active surfaces have difficulties progressing into concave boundary regions [3]. There is currently no satisfactory solution to this problem, although pressure forces [13], control points [3], adding nodes [14], and using solenoidal external fields [5] have been proposed.

A 2D example of the second problem is shown in Figs. 2a-c. Fig. 2a shows a line drawing of a U-shaped object having a concave region (as viewed from the outside) at the top of the figure, and Fig. 2c shows a sequence of curves depicting the iterative progression of a traditional active contour toward the boundary. The final solution satisfies the Euler equations of the active contour formulation, but remains split across the concave region. The reason for the poor convergence is revealed in Fig. 2b, where the external field for this example, is depicted. Although the field correctly points toward the object boundary, in the concave portion the forces point horizontally *in opposite directions*. Thus, the curve is "pulled" apart toward the U-shape, but not made to progress downward into the concave region. This poor performance lies in the problem formulation, not its method of solution.

3.2 A New Active Surface Model

Since the ability to find an object boundary using an active surface is largely controlled by the external force term, we have started from the force balance equation (5) with the goal of replacing the traditional external force with a new type of external force. This new external force should

- pull an active surface towards the object boundary even when the surface is far away,
- pull the active surface into concave regions, and
- vary smoothly in homogeneous regions.

In [6], we have defined a vector field $\mathbf{v}(\mathbf{x})$, called the *gradient vector flow* (GVF) field, that meets the above properties. The GVF field is a vector field $\mathbf{v}(\mathbf{x})$ that minimizes the following energy functional

$$\mathcal{E} = \int \mu|\nabla \mathbf{v}|^2 + |\nabla f|^2 \, |\mathbf{v} - \nabla f|^2 d\mathbf{x} \tag{7}$$

where the gradient operator ∇ is applied to each component of $\mathbf{v}$ separately, $f(\mathbf{x}) = -E_{ext}(\mathbf{x})$, and $E_{ext}(\mathbf{x})$ can be computed either using equation (2) or (3) (other choices are also possible (cf. [6])).

According to this model, when $|\nabla f|$ is large, i.e, near the edge, the second term dominates the integrand, and is minimized by setting $\mathbf{v} = \nabla f$. On the other hand, when $|\nabla f|$ is small, the energy is dominated by partial derivatives of the vector field, yielding a smooth field. This also extends the vector field to regions far away from the edge. The parameter μ is a regularization parameter governing the tradeoff between the first term and the second term. This parameter should be set according to the amount of noise present in the image (for more noise, increase μ).

Using the calculus of variations, we find that the GVF field must satisfy the vector Euler equation

$$\mu\nabla^2\mathbf{v} - (\mathbf{v} - \nabla f)|\nabla f|^2 = \mathbf{0} \tag{8}$$

where ∇^2 is applied to each component of the vector field $\mathbf{v}$ separately. A solution to this equation can be found by introducing a time variable t and finding the steady-state solution of the following linear parabolic partial differential equation

$$\mathbf{v}_t = \mu\nabla^2\mathbf{v} - (\mathbf{v} - \nabla f)|\nabla f|^2 \tag{9}$$

where $\mathbf{v}_t$ denotes the partial derivative of $\mathbf{v}$ with respect to t. Equation (9) comprises three decoupled scalar linear second order parabolic partial differential equations in each element of $\mathbf{v}$. Therefore, in principle, it can be solved in parallel. It was shown in [6] that Equation (9) can be solved iteratively using an explicit finite difference scheme. The stability and convergence of this iterative algorithm is guaranteed when the spatial finite difference

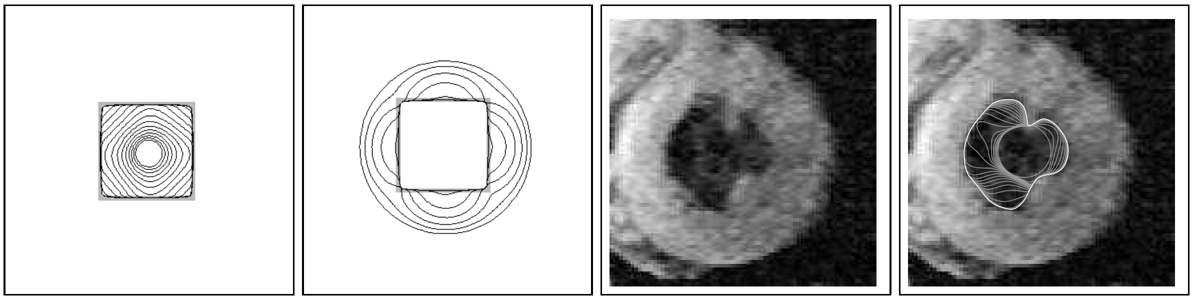

Figure 3: (a) and (b) A GVF active contour converges to the desired boundary regardless of whether it is initialized inside or outside. (c) A magnetic resonance image of the left ventrical of a human heart (short-axis section). (d) Initial and intermediate contours (gray curves) and the final contour (white curve) of the GVF active contour.

spacing Δx, Δy, and Δz in each dimension as well as the time step Δt for each iteration satisfy the following condition

$$\Delta t \leq \frac{\Delta x \Delta y \Delta z}{6\mu} \tag{10}$$

After $\mathbf{v}(\mathbf{x})$ is computed, we replace the potential force $-\nabla E_{\text{ext}}(\mathbf{x})$ in the dynamic active surface equation of (6) by $\mathbf{v}(\mathbf{x})$, yielding

$$\mathbf{x}_t = \alpha \nabla^2_{\mathbf{u}} \mathbf{x} - \beta \nabla^2_{\mathbf{u}} (\nabla^2_{\mathbf{u}} \mathbf{x}) + \mathbf{v} \tag{11}$$

We call the surface evolving according to the above dynamic equation a *GVF active surface*. This equation is solved in a similar fashion to the traditional active surface — i.e., by discretization and iterative solution. The *GVF active contour*, a parameterized curve in 2D, can be defined in analogous fashion (cf. [6]).

3.3 Results

In Fig. 2e, a GVF active contour is shown to move into the concave region where the traditional active contour failed. The corresponding GVF field is shown in Fig. 2d. Notice that the initial position of the GVF active contour is farther away from the object than the initialization in Fig. 2c, yet it still converges to the desired boundary. This result can be explained by comparing the GVF field with the traditional external force field (Fig. 2b). First, in regions far away from the object boundary, the GVF field has vectors pointing towards the boundary where the traditional external force field does not. Second, in concave regions (either viewed from outside or inside the U shape), the GVF field has vectors pointing into the concave region boundary where the vectors of traditional external force field point sideways.

Figs. 3a and 3b show that the GVF active contour converges to the desired boundary regardless of whether it is initialized inside or outside the object boundary. Fig.3c shows a magnetic resonance image (short-axis section) of the left ventricle of a human heart. Fig.3d

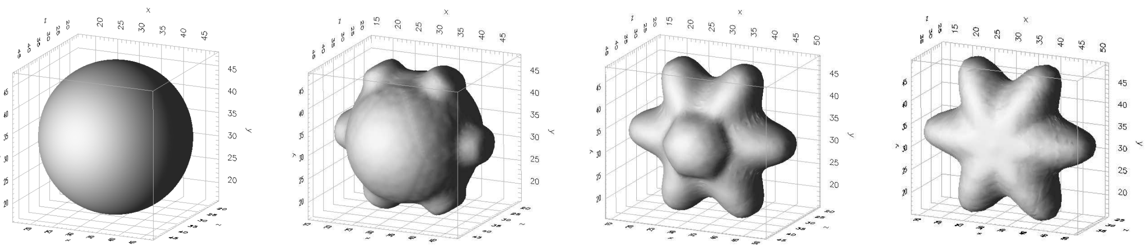

(a) (b) (c) (d)

Figure 4: (a) Initial configuration of the GVF active surface and its positions after (b) 10, (c) 40, and (d) 100 iterations.

shows a sequence of GVF active contours (plotted in a shade of gray) and the GVF active contour result (plotted in white). Clearly, many details on the endocardial borders are captured by the GVF active contour result, including the papillary muscles (the bumps that protrude into the cavity).

In Fig. 4, a GVF active surface is initialized as the sphere shown in Fig. 4a, which is neither entirely inside nor outside a three-dimensional star-shaped object. The GVF active surface evolves according to (11), and intermediate results after 10 and 40 iterations are shown in Fig. 4b and c. The final result after 100 iterations is shown in Fig. 4d.

4 Cortical Surface Reconstruction

We now summarize our initial efforts on cortical surface reconstruction from 3D MR images. To prepare the data, the acquired MR images were stacked to form a volume and then preprocessed to remove skin, bone, fat, and other extracranial tissue using a semi-automated software package[1]. A fuzzy c-means segmentation program[2] was then used to segment the image volumes, resulting in fuzzy membership functions for gray matter (GM), white matter (WM), and cerebrospinal fluid (CSF). As a first attempt, we tried to initialize a GVF active surface as a sphere and apply it to the segmented data. The human cortex, however, is so convoluted that even a GVF active surface can not find the complete cortex from this simple initialization. In order to obtain a better estimate, a better initial surface is needed.

To address this problem, we presented in [9] a method using an *isosurface* algorithm over the computed WM membership function. An isosurface is a surface that passes through all locations in space where a continuous data volume is equal to a constant value. The construction of isosurfaces is a well-studied problem [15, 16]. The surface produced by an isosurface algorithm, however, does not have any constraint on its topology. When noise or partial volume averaging artifacts corrupt the data, the resulting surface may have a different topology from the topology of the true object boundary. Since an active surface ordinarily does not change its topology, a topologically correct initialization is needed.

[1]Developed by Christos Davatzikos and Jerry Miller, Department of Radiology, Medical School, JHU.
[2]Developed by Dzung Pham, Image Analysis and Communication Lab, JHU-ECE.

# *Vertices*	χ	# *meshes*
356,814	−462	1
178	2	1
51 – 124	2	6
21 – 50	2	45
6 – 20	2	507

(a)

# *iterations*	χ
0	−462
1	−26
2	−12
3	−6
4	0
5	2

(b)

Table 1: (a) Euler characteristic of resulting surface after each iteration, (b) Size and Euler characteristics of meshes from original isosurface.

The topology of a surface can be summarized by its Euler characteristic, χ, which can be computed by [17]

$$\chi = V - E + F \tag{12}$$

where V is the number of vertices, E is the number of the edges, and F is the number of faces. A value of χ equal to two indicates that the surface is topologically equivalent to a sphere. The existence of handles (like that of a coffee cup) in the surface reduces the value of χ [18]. We found that handles on the surface could be removed by performing successive median filters on the WM tissue data and recomputing the isosurface.

In addition to the topology problem, the output from an isosurface algorithm on the WM membership function data usually contains many small meshes which correspond to voxels that have been corrupted by noise and other artifacts. These meshes are physically not connected to the real WM outer surface. We therefore designed an efficient algorithm that separates the meshes by their vertex connectivity and outputs only the largest mesh.

Our automatic procedure for computing an initial estimate of the cortical surface can be summarized as follows:

1. Compute an isosurface on the WM membership function data.

2. Extract only the connected surface with the largest number of vertices.

3. Compute χ.

4. If χ is not equal to 2, then apply a median filter to the WM membership function, recompute the isosurface on the filtered data, and go to Step 2.

Median filtering was performed using a 3×3×3 kernel. Table 1a shows the number of surfaces and their χ values before any median filtering has taken place. The one mesh which is clearly much larger than all other meshes represents a topologically incorrect estimate of the GM-WM interface. Table 1b shows how the χ of the resulting surface increases after each iteration and eventually converges to the desired value of two. The estimated initial surface is shown in Fig. 5a.

An initial estimate of the cortical surface computed in this manner is a smoothed estimate of the GM/WM interface. We then used an edge map f computed on the GM membership

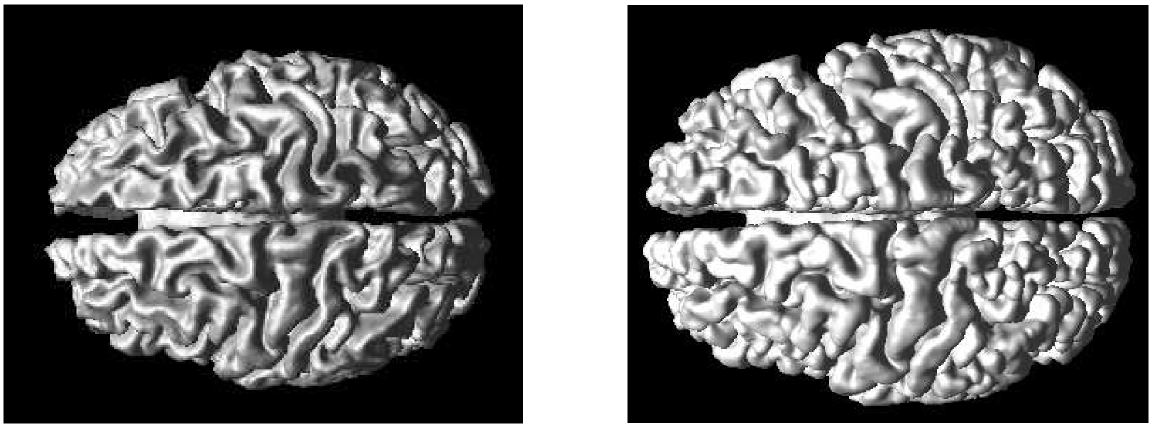

(a) (b)

Figure 5: (a) topologically correct initial surface estimate. (b) Reconstructed cortical surface.

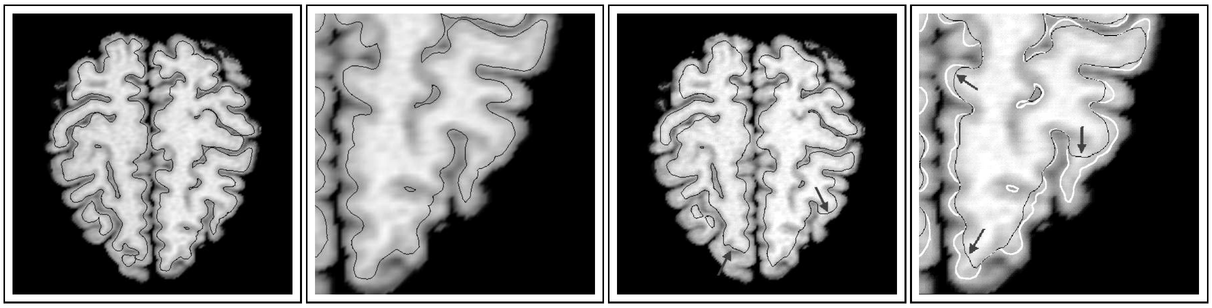

(a) (b) (c) (d)

Figure 6: MRI images overlaid with reconstructed cortical surface (a)-(b) using GVF, and (c)-(d) using traditional external forces. Arrows in (c)-(d) indicate the samples of where the traditional force has poor performance.

function to generate a GVF field that attracted a GVF active surface starting from the above estimated initial position to the middle layer of the cortex. Fig. 5b shows the final result of a GVF active surface on our sample data set. The final GVF active surface is bigger than the initial estimate because the GVF active surface grows outwards and stabilizes at the middle layer of GM. Fig. 6a shows a cross-section with the final GVF active surface superimposed on an axial MR slice. Fig. 6b shows a magnified region of the same slice. For comparison, results using traditional gradient force with the same initialization are shown in Figs. 6c-d. The corresponding GVF result is also plotted as white in Fig. 6d. Arrows in Fig. 6c-d indicate the sample areas where the traditional external force had poor performance. These figures show that the performance of our proposed method is superior to the traditional active surface. They also show that most of the complex sulci and gyri were reconstructed by the GVF active surface. However, some structures still were not fully found. We are now investigating further improvements to these results.

5 Differential Geometry Computation of Cortical Surface

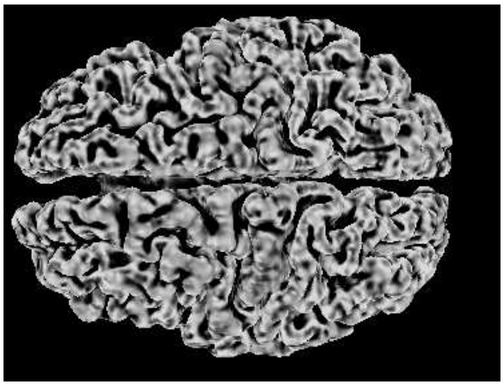

Figure 7: Mean curvature plotted on the reconstructed cortical surface.

Once the cortex has been identified using the method described in Section 3, differential geometric quantities may be computed. Differential geometry provides a natural mathematical framework to study the cortical surface geometry. Among many geometric quantities defined for the surface, curvature information is the most valuable since it quantifies the structure of the sulci and gyri, thus providing the basis for scientific and comparative studies.

The fundamental quantities for describing surface curvature are maximum and minimum principal curvatures. Maximum and minimum principal curvatures describe the maximum and minimum degree of the surface curving away or towards the normal direction at a surface point. Mean curvature, the average of the principal curvatures, takes on positive values at valleys and troughs and negative values at ridges and peaks. Gaussian curvature, the product of two principal curvatures, takes on positive values at peaks and negative values at troughs. These quantities serve as geometry descriptors which are independent of the surface parameterization.

We developed an algorithm to compute the maximum principal, minimum principal, mean, and Gaussian curvatures based on the simplex mesh surface representation. In order to estimate the curvatures on the discretized mesh, we fit a quadratic surface patch to a small neighborhood around each vertex. Then we compute all the curvatures for the quadratic surface (cf., [19]) and use them as curvature estimates for the discrete mesh.

Fig. 7 shows the mean curvature plotted on the reconstructed cortical surface of our sample data set. Black in the mean curvature figure stands for negative mean curvature values, grey stands for zero, white stands for positive mean curvature values.

6 Discussion and Future Work

In conclusion, we have proposed a new class of external force models for active surfaces/contours called GVF which largely solves two problems associated with traditional active surfaces/contours. We also developed a method which incorporates GVF active surfaces, fuzzy segmentation, and isosurface algorithm which yields some promising results in cortical surface reconstruction. The main drawback of this method, however, is that we do not know whether the WM isosurface, under the successive median filtering, will always converge the desired topology. A theoretical analysis of justifying the use of median filters is currently underway as well as an investigation of other methods for initializing the GVF active surface.

Once we have obtained an accurate cortical surface, possible directions for our future work are

1. brain geometry analysis using differential geometry,
2. a cortical surface flattening algorithm,
3. functional MRI mapping onto the reconstructed cortical surface,
4. brain registration based on functional MRI and cortical geometry.

7 Acknowledgments

I would like to thank Dr. J. L. Prince for his invaluable guidance and continued support for this work. This proposal rests on some key results obtained from the Ph.D. dissertation of Dr. Christos Davatzikos. I am grateful for his help during the course of this investigation. I also take this opportunity to thank Dr. R. N. Bryan, Dzung Pham, and Sandeep Gupta for their help and support in this work. This work was supported by NSF grant MIP-9350336.

REFERENCES

[1] S. Sandor and R. Leahy. Towards automated labelling of the cerebral cortex using a deformable atlas. In *Information Processing in Medical Imaging*, pages 127–138, 1995.

[2] D. MacDonald, D. Avis, and A. C. Evans. Multiple surface identification and matching in magnetic resonance images. In *SPIE Proc. VBC '94*, volume 2359, pages 160–169, 1994.

[3] C. A. Davatzikos and J. L. Prince. An active contour model for mapping the cortex. *IEEE Trans. Med. Imag.*, 14(1):65–80, March 1995.

[4] C. Davatzikos and R. N. Bryan. Using a deformable surface model to obtain a shape representation of the cortex. *IEEE Trans. Med. Imag.*, 15, Dec. 1996. To appear.

[5] J. L. Prince and C. Xu. A new external force model for snakes. In *1996 Image and Multidimensional Signal Processing Workshop*, pages 30–31, 1996.

[6] C. Xu and J. L. Prince. Snakes, shapes, and gradient vector flow. Submitted for publication in *IEEE Transactions on Image Processing* (Tech. Rep. JHU/ECE 96-15).

[7] C. Xu and J. L. Prince. Gradient vector flow: A new external force for snakes. Submitted for publication in CVPR-97.

[8] C. Xu and J. L. Prince. A generalized gradient vector flow for active contour models. In *1997 Conf. Info. Sci. Syst., Johns Hopkins University*, March 1997. To appear.

[9] C. Xu, , D. L. Pham, and J. L. Prince. Finding the brain cortex using fuzzy segmentation, isosurfaces, and deformable surface models, 1997. To appear in *the XVth International Conference on Information Processing in Medical Imaging* (Tech. Rep. JHU/ECE 96-17).

[10] R. Courant and D. Hilbert. *Methods of Mathematical Physics*, volume 1. Interscience, New York, 1953.

[11] H. Delingette. Adaptive and deformable models based on simplex meshes. In *Proceedings of the 1994 IEEE Workshop on Motion of Non-Rigid and Articulated Objects*, pages 152–157, 1994.

[12] M. Kass, A. Witkin, and D. Terzopoulos. Snakes: Active contour models. *International Journal of Computer Vision*, 1(4):321–331, 1987.

[13] L. D. Cohen. On active contour models and balloons. *CVGIP: Image Understanding*, 53(2):211–218, March 1991.

[14] S. Lobregt and M. A. Viergever. A discrete dynamic contour model. *IEEE Trans. Med. Imag.*, 14(1):12–24, March 1995.

[15] W. E. Lorensen and H. E. Cline. Marching cubes: A high-resolution 3D surface construction algorithm. *ACM Comp. Graph.*, 21(4):163–170, 1987.

[16] C. Montani, R. Scateni, and R. Scopigno. Discretized marching cubes. In *IEEE Proc. Visualization'94*, pages 281–287, 1994.

[17] M. K. Agoston. *Algebraic Topology — A first course.* Marcel Dekker, Inc., New York, 1976.

[18] A. van Gelder and J. Wilhelms. Topological considerations in isosurface generation. *ACM Trans. on Graphics*, 13:337–375, 1994.

[19] R. S. Millman and G. D. Parker. *Elements of Differential Geometry.* Prentice-Hall, Inc., Englewood Cliffs, 1977.